

Communication

# Molecular Mechanism of Cyanidin-3-O-Glucoside Disassembling A $\beta$ Fibril In Silico

Jihui Gao, Jiahui Fu, Xiaoyu Gao and Dong Yang \* 

Beijing Key Laboratory of Functional Food from Plant Resources, College of Food Science & Nutritional Engineering, China Agricultural University, 17 East Tsinghua Rd., Beijing 100083, China

\* Correspondence: dyang@cau.edu.cn

**Abstract:** The deposition of  $\beta$ -amyloid (A $\beta$ ) in the brain leads to neurotoxic effects and subsequent Alzheimer's disease (AD). While AD is becoming more and more prevalent in modern society, therapeutic efforts targeting A $\beta$  could be a promising solution. Currently, two natural products are reported to disintegrate preformed A $\beta$  fibril in vitro. Meanwhile, the chemical driving force behind this phenomenon remains unknown. Taking cyanidin-3-O-glucoside (Cy-3G) as an example, here we studied its interaction with different A $\beta$  polymorphs in silico. Negative charges on different A $\beta$  polymorphs draw the interaction with the flavylium cation on Cy-3G. Our results show that A $\beta$  in a single peptide form in solution exposed more hydrophobic solvent accessible surface area than its fibril structure (per protomer), and Cy-3G interacts more intensively with the single peptide form than fibril as indicated by more hydrogen bonding formed and more amino acid residues involved in their hydrophobic interactions. Thus, the single A $\beta$  peptide aggregation into fibril and fibril dissociation into single peptide equilibrium could be disturbed by the preferential binding of Cy-3G to the monomeric A $\beta$  peptide, which leads to the disassembly of the pathogenic A $\beta$  fibril. This study offers a novel perspective of Cy-3G alleviated AD syndrome beyond its dogmatic antioxidant activity.

**Keywords:** A $\beta$ ; fibril; disassembly; cyanidin-3-O-glucoside; Alzheimer's disease



**Citation:** Gao, J.; Fu, J.; Gao, X.; Yang, D. Molecular Mechanism of Cyanidin-3-O-Glucoside Disassembling A $\beta$  Fibril In Silico. *Nutrients* **2023**, *15*, 109. <https://doi.org/10.3390/nu15010109>

Academic Editor: Panteleimon Giannakopoulos

Received: 29 November 2022

Revised: 18 December 2022

Accepted: 23 December 2022

Published: 26 December 2022



**Copyright:** © 2022 by the authors. Licensee MDPI, Basel, Switzerland. This article is an open access article distributed under the terms and conditions of the Creative Commons Attribution (CC BY) license (<https://creativecommons.org/licenses/by/4.0/>).

## 1. Introduction

Alzheimer's disease, the most prevalent aging-related dementia, has become increasingly common in modern society [1]. The deposition of A $\beta$  in the brain and subsequent neuron and synaptic loss has been the character of AD for almost 30 years [2]. Unfortunately, therapies targeting A $\beta$  have not proved their efficacy in preventing AD progression and have raised many doubts [3,4]. However, the recent approval of aducanumab possibly restrengthenes the validity of curing AD via targeting A $\beta$  [5]. With emerging targets against AD, it may evolve into a multifactorial disease with multiple therapeutic sites [6,7]. Interestingly, naphthoquinone and anthraquinone derivatives could target different sites in AD with similar structure scaffolds [8].

Two major types of A $\beta$  peptides are involved in AD, A $\beta$ <sub>40</sub> and A $\beta$ <sub>42</sub>, and the amino acid sequence of the latter is that of the former with two more residues at the C-terminus [9]. Although the total concentration of A $\beta$ <sub>40</sub> is higher than that of A $\beta$ <sub>42</sub>, the latter is the major peptide species in parenchymal plaques [10–12]. Additionally, the A $\beta$ <sub>40</sub> fibril prepared in vitro adopts different morphologies, including straight fibrils and twisted morphology [13–15]. The irrelevancy of the A $\beta$ <sub>40</sub>-related pathology and the ambiguity of its structural morphology has rendered this peptide to be studied less than others. On the other hand, oligomeric A $\beta$ <sub>42</sub> not only exhibits neurotoxicity but also induces mature fibril formation as the hallmark of AD [16,17]. Thus, halting the formation of A $\beta$ <sub>42</sub> oligomers and subsequent fibril formation is the key to retarding AD progression.

Many natural products, such as polyphenols and flavonoids, exhibit alleviating effects against AD [18,19]. While the exact mechanisms of their function remain unknown, researchers are trying to link the dogmatic antioxidative property of these molecules to their

neuroprotective effect [20,21]. Cy-3G exhibits not only anti-tumor and anti-inflammatory activities [22,23] but also neuroprotective effects in cells and rats [24–26]. Recently, Liu et al. showed that Cy-3G reduced the amount of intracellular reactive oxygen species induced by A $\beta$ <sub>40</sub> fibrillogenesis [27]. Furthermore, Cy-3G was found to prevent A $\beta$ <sub>40</sub> fibrillogenesis and disintegrate its pre-formed fibrils [27]. While Cy-3G is shown to pass the blood–brain barrier and rapidly distribute in the brain, whether Cy-3G could inhibit fibrillogenesis of the more pathologically relevant A $\beta$ <sub>42</sub> peptide remains unknown [28]. Besides the fact that Cy-3G interacts with the preformed fibril with hydrophobic and electrostatic interactions, the chemical process that drives the disassembly of A $\beta$ <sub>40</sub>, or the more pathologically relevant A $\beta$ <sub>42</sub> fibril, remains unclear.

Here, based on the experimental evidence that Cy-3G inhibits both the A $\beta$  fibrillogenesis and interacts with the A $\beta$  fibril, we studied the detailed interaction between monomeric and fibrillar A $\beta$  with Cy-3G *in silico*. The analysis of Cy-3G interacting with different A $\beta$ <sub>42</sub> polymorphs revealed the chemical driving force of Cy-3G induced A $\beta$  fibril disassembly.

## 2. Materials and Methods

### 2.1. Molecule Preparation

The Cy-3G structure was generated with ChemDraw Pro. 18.0 (CambridgeSoft, Cambridge, MA, USA). AD-relevant solid-state NMR structure of A $\beta$ <sub>42</sub> (PDB ID: 2NAO) was used to simulate Cy-3G binding to fibrillar A $\beta$  [29].

For monomeric A $\beta$ , one peptide of the above fibrillar structure was derived with PyMol (Schrödinger, New York, NY, USA) and subjected to protein preparation with the BIOVIA Discovery Studio software V16.1.0. The monomeric A $\beta$  was prepared with CHARMM minimization and protonated with a dielectric constant of 10. The pH was set to 7.5, and the ionic strength was set to 0.08. In the following solvation step, 2593 water molecules, 7 sodium and 4 chloride ions were added to neutralize monomeric A $\beta$  using the explicit periodic boundary water model in an orthorhombic cube with a radius of 20 Å and a minimum distance from a boundary of 7.0 Å. The monomeric A $\beta$  was obtained by simulating the standard dynamics cascade with two energy minimization steps. Firstly, 1000 steps of steepest descent minimization and 2000 steps of conjugate gradient minimization, followed by steps of heating, equilibration and production. The monomeric A $\beta$  system was heated from 50 K to 310.15 K in 4 ps with a time step of 2 fs, and equilibrated at 310.15 K for 20 ps with a time step of 2 fs. The SHAKE constraint on hydrogen atoms is applied. Finally, the production step was run at 310.15 K for 200 ps with a time step of 2 ps typed NPT [30].

### 2.2. Molecule Interaction

The molecular interaction between Cy-3G and monomeric, fibrillar A $\beta$  polymorph was performed with the DS CDocker module. Random ligand conformations were generated from the initial ligand structure through high-temperature molecule dynamics at 1000 K. The random ligand conformations were refined by grid-based simulated annealing with 2000 steps heating to 700 K and 5000 steps cooling to 300 K and force field minimization. The top 10 poses were saved for subsequent analysis.

### 2.3. Analysis

For Cy-3G to interact with the monomeric and fibrillar A $\beta$  polymorph, the conformation with the lowest energy was selected for molecular interaction analysis. LigPlot (EMBL-EBI Groups, Cambridgeshire, UK) and PyMol were used to analyze the electrostatic, hydrophobic interactions and hydrogen bonding, respectively [31].

## 3. Results

### 3.1. Simulated Single A $\beta$ peptide Solution Structure

In 2020, Cy-3G and amentoflavone were sequentially reported disassembling pre-formed A $\beta$  fibril [27,32]. Our previous microscale thermophoresis experiment indicated

that cyanidin-3-*O*-galactoside preferentially binds to the monomeric A $\beta$  than its fibril polymorph. To investigate whether Cy-3G also exhibits preferential binding to monomeric A $\beta$ , we simulated the solution structure of a single A $\beta$  peptide first. The results showed that a single A $\beta$  exhibited a majorly unfolded structure, with a bent turn structure from F19 to I32, consistent with the previous simulation of A21 to A30 truncate structure and NMR results (Figure 1a) [33,34]. The solvent accessible surface area (SASA) of the hydrophobic region in the 6-peptide A $\beta$  fibrillar polymorph is 4835.67 Å<sup>2</sup>, while in one A $\beta$  peptide is 2318.76 Å<sup>2</sup>. The monomeric A $\beta$  peptide alone exposed more hydrophobic surface area in solution than its aggregated fibrillar polymorph.

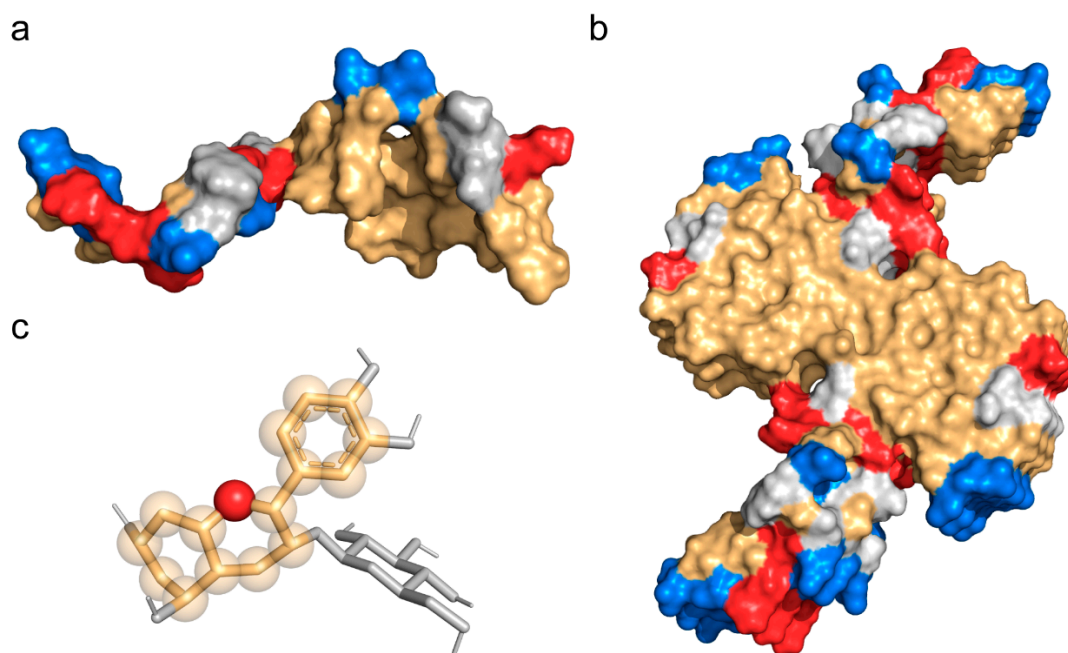


**Figure 1.** Structure of Cy-3G and different A $\beta$  polymorph. (a) Space-filling model of a simulated, single A $\beta$  peptide solution structure. Positive and negative charges on the proteins are shown in tv\_red and marine, respectively. The hydrophobic part is shown in light orange. (b) Space-filling model of a disease-relevant A $\beta$  fibril structure. (c) Space-filling model of Cy-3G showing the positive charge (tv\_red) and the hydrophobic character (light orange) on the 2-phenylbenzopyrylium core of this molecule.

There is a negative charge on the bulk hydrophobic region of the single A $\beta$  peptide from the deprotonation of E22 and D23 (Figure 1a). Similarly, the fibrillar A $\beta$  structure exhibits large proportions of hydrophobic core regions with negative and positive charges on its sides (Figure 1b). On the contrary, the molecular structure of Cy-3G is a hydrophobic core carrying a positive flavylium cation (Figure 1c).

### 3.2. Interaction between A $\beta$ Fibril and Cy-3G

Interestingly, the CDOCK of Cy-3G to the fibrillar A $\beta$  polymorph revealed two different binding sites (Figure 2a). As defined previously, one binding site is at the hydrophobic core of one A $\beta$  stack composed of peptide D-F in the fibril [29]. In the first binding site, Cy-3G formed hydrogen bonds with G9, E11, V12, and H13 in peptide chain E, and hydrophobic interactions with G9, E11, H13, F4, and H6 in peptide chain E, H6 and Y10 in chain D, and H6 and G9 in chain F (Figure 2b). The CDOCKER interaction energy between Cy-3G and this site is  $-181.31$  kJ/mol (Table 1).

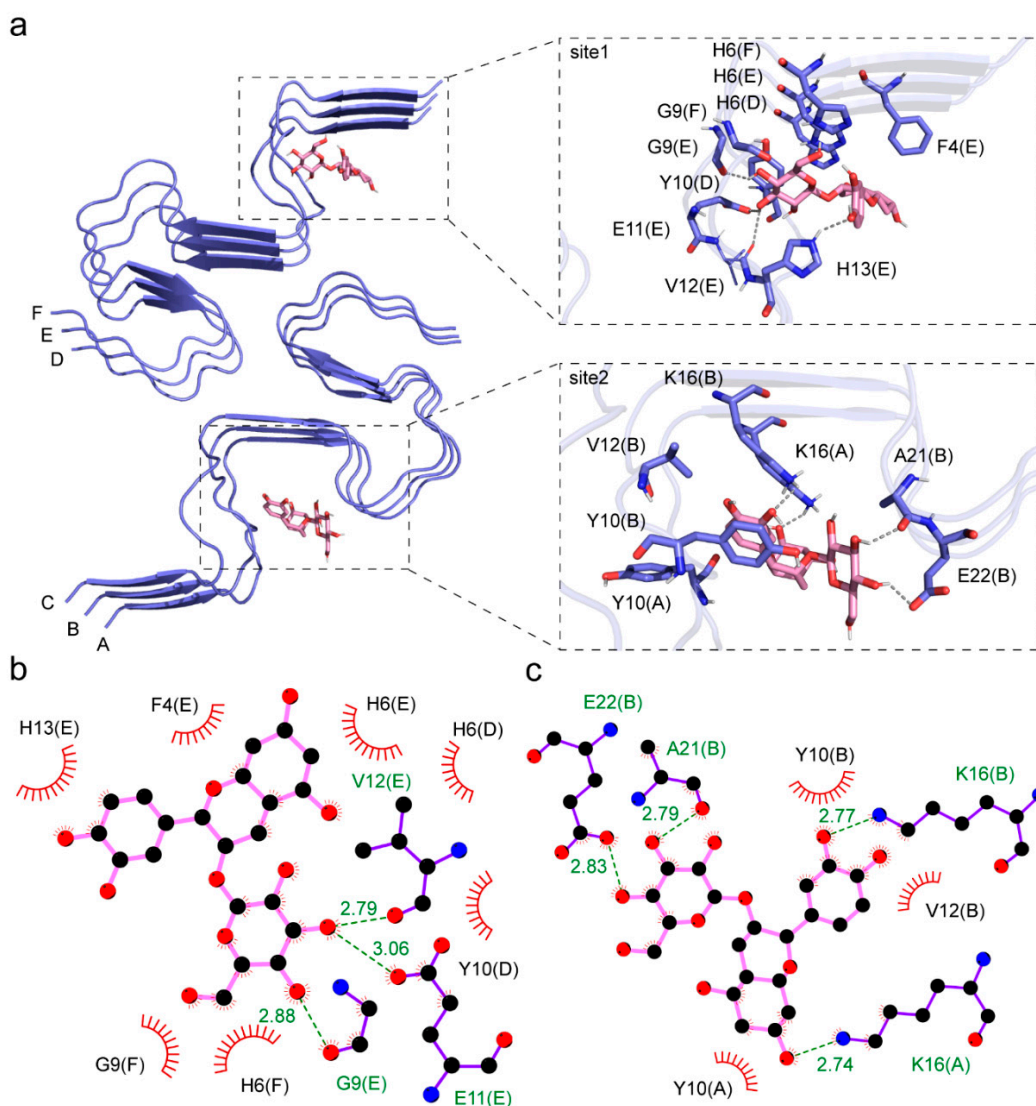


**Figure 2.** The interaction between Cy-3G and the Aβ fibril. (a) The two binding sites between Cy-3G and a disease-relevant Aβ fibril. The cartoon representation is the Aβ fibril structure, and the pink stick presentation is the Cy-3G molecule. The first binding site is the hydrophobic core of one fibril stack, and the other binding site is on the opposite side of the hydrophobic site. (b,c) are the interaction details between Cy-3G and the first and second binding sites. The dashed lines represent hydrogen bonding, and amino acid residues involved in hydrophobic interactions were shown. For example, F4(E) indicates the fourth phenylalanine in Chain E of the Aβ fibril.

**Table 1.** Binding parameters of Cy-3G to different Aβ polymorphs.

Aβ Polymorph	CDOCKER Interaction Energy (kJ/mol)	Number of Hydrogen Bonds	Number of Amino Acid Residues Involved in Hydrophobic Interactions
Single peptide	−43.29	4	11
Fibril site1	−181.31	4	9
Fibril site2	−197.72	4	7

The other binding site is at the opposite side of the hydrophobic core in the other Aβ stack of the fibril composed of peptide A-C. Here, Cy-3G formed a hydrogen bond with K16 in peptide chain A, K16, A21, and E22 in peptide chain B, and hydrophobic interactions with K16, Y10 in peptide chain A, K16, A21, E22, Y10, and V12 in peptide

chain B (Figure 2c). The CDOCKER interaction energy between Cy-3G and this site is  $-197.72$  kJ/mol (Table 1).

### 3.3. Interaction between a Single A $\beta$ Peptide and Cy-3G

When Cy-3G binds to a single A $\beta$  peptide, there is only one binding site at the major hydrophobic region (Figure 3a). Here, Cy-3G forms hydrogen bonds with F19, A21, D23, and G25, and hydrophobic interactions with F19, A21, D23, G25, V18, F20, E22, V24, A30, I31, and I32 (Figure 3b). The CDOCKER interaction energy between the Cy-3G and a single A $\beta$  peptide is  $-43.29$  kJ/mol (Table 1).

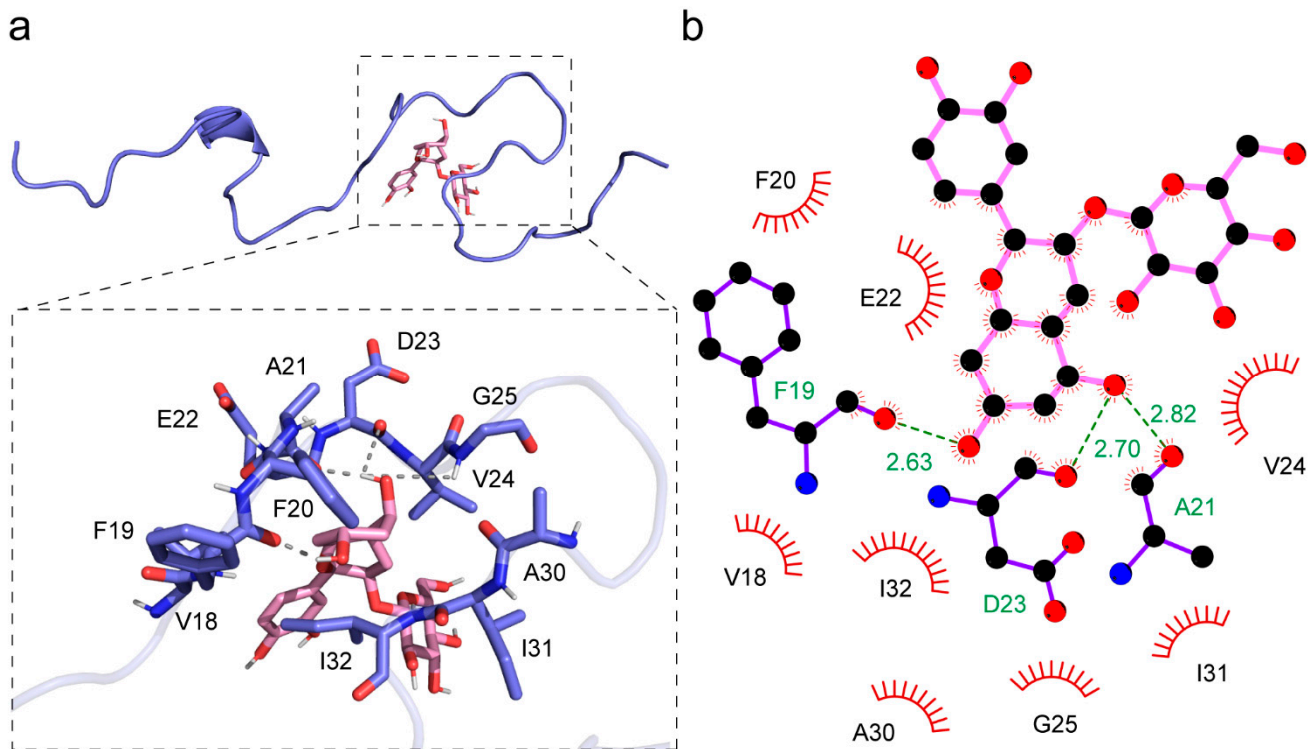


**Figure 3.** Detailed interaction between Cy-3G and an A $\beta$  peptide. (a) The binding site between Cy-3G and an A $\beta$  peptide. The slate carton representation is the A $\beta$  peptide solution structure, and the pink stick presents Cy-3G. (b) The interaction details between Cy-3G and the A $\beta$  peptide. The dashed lines represent hydrogen bonding, and amino acid residues involved in hydrophobic interactions were shown.

### 3.4. Preferential Binding of Cy-3G to a Single A $\beta$ Peptide over the Fibrillar Polymorph

It is observed that the monomeric A $\beta$  peptide solution structure exhibits a larger SASA of hydrophobic area. This character draws the interaction between the similarly hydrophobic core of Cy-3G and different A $\beta$  polymorphs. Another significant molecular characteristic between Cy-3G and both A $\beta$  polymorphs is the electric charge they carry. Cy-3G carries a positive flavylium cation on its 2-phenylbenzopyrylium hydrophobic core, and it is this positive charge that drives this small molecule to bind to the region of each A $\beta$  polymorph with negative charges. The detailed consequences of this charge–charge interaction are not discussed here due to limited computational work.

Clearly, Cy-3G interacts with a single A $\beta$  peptide more intensively than the fibrillar polymorph. There are four hydrogen bonds between Cy-3G and A $\beta$  fibril at each binding site, while there are also four hydrogen bonds between Cy-3G and the single A $\beta$  peptide (Table 1). Considering there are six A $\beta$  peptides in one fibril structure studied here, there are more hydrogen bonds formed between Cy-3G and a single A $\beta$  peptide than its fibril polymorph.

In contrast, 11 amino acid residues are involved in the hydrophobic interactions between Cy-3G and a single A $\beta$  peptide. At the same time, the number decreased to 9 when Cy-3G binds to the first site of the A $\beta$  fibril and 7 when Cy-3G binds to the second site (Table 1). There is a much more intensive hydrophobic interaction between Cy-3G and a single A $\beta$  peptide than its fibril polymorph. Thus, Cy-3G preferentially binds to the monomeric single A $\beta$  peptide than the fibril. A $\beta$  peptides aggregate into fibrils and fibrils dissociate into a single peptide; in this chemical equilibrium, pathology favors the aggregation side. In the presence of Cy-3G preferential binding to the single A $\beta$  peptide, this chemical equilibrium could be driven to the side of disassembling of A $\beta$  fibril into its single peptide polymorph. Specifically, the binding of Cy-3G to the F19 and the I32 turn structure fulfills the prediction of a drug candidate targeting this region [34]. Our research only demonstrates a thermodynamic phenomenon, while future stoichiometry studies are needed for the pharmaceutical application of this compound.

This study differs from previous simulations performed on the trimer of A $\beta$ 40 and was performed with two different A $\beta$ 42 structures: the monomeric, free in solution form, and the hexameric, fibrillar form [27]. As A $\beta$ 42 is more AD-relevant than A $\beta$ 40, the A $\beta$  fibrillar structure employed in this study is also more relevant to the disease [29]. Here, we found that Cy-3G disrupts the core structure of A $\beta$  fibril, as indicated in the previous study [27], and illustrated its preferential binding to the monomeric A $\beta$  that offers a thermodynamic explanation of this phenomenon.

#### 4. Conclusions

The positive charge of the flavylum cation on Cy-3G draws the interaction between this molecule and the negative charges on different A $\beta$  polymorphs. The simulated A $\beta$  single-peptide polymorph displays a larger hydrophobic SASA than its fibril structure, enabling a more intensive interaction between Cy-3G and the hydrophobic region. Thus, the Cy-3G preferentially binds to the single A $\beta$  peptide than its fibril polymorph. The A $\beta$  aggregation/dissociation equilibrium exists between its single peptide and fibril polymorph. It could be the preferential binding of Cy-3G to the single peptide that drives the equilibrium to the dissociation direction, which eventually leads to the disassembling of A $\beta$  fibril.

**Author Contributions:** Conceptualization, D.Y.; Methodology, J.G., J.F. and X.G.; Software, J.G., J.F. and X.G.; Writing—original draft, D.Y.; Writing—review and editing, J.G. All authors have read and agreed to the published version of the manuscript.

**Funding:** This research is supported by the National Laboratory of Biomacromolecules, Chinese Academy of Sciences, grant number 2022kf05.

**Institutional Review Board Statement:** Not applicable.

**Informed Consent Statement:** Not applicable.

**Data Availability Statement:** Data is contained within the article.

**Acknowledgments:** The authors are grateful to Chih-chen Wang in the Institute of Biophysics, Chinese Academy of Sciences, for her support and encouragement in our research.

**Conflicts of Interest:** The authors declare no conflict of interest.

#### References

1. Dartigues, J.F. Alzheimer's disease: A global challenge for the 21st century. *Lancet Neurol.* **2009**, *8*, 1082–1083. [[CrossRef](#)] [[PubMed](#)]
2. Hardy, J.A.; Higgins, G.A. Alzheimer's disease: The amyloid cascade hypothesis. *Science* **1992**, *256*, 184–185. [[CrossRef](#)] [[PubMed](#)]
3. Servick, K. Doubts persist for claimed Alzheimer's drug. *Science* **2019**, *366*, 1298. [[CrossRef](#)]
4. Mullane, K.; Williams, M. Alzheimer's disease beyond amyloid: Can the repetitive failures of amyloid-targeted therapeutics inform future approaches to dementia drug discovery? *Biochem. Pharmacol.* **2020**, *177*, 113945. [[CrossRef](#)] [[PubMed](#)]
5. Sevigny, J.; Chiao, P.; Bussiere, T.; Weinreb, P.H.; Williams, L.; Maier, M.; Dunstan, R.; Salloway, S.; Chen, T.; Ling, Y.; et al. The antibody aducanumab reduces Abeta plaques in Alzheimer's disease. *Nature* **2016**, *537*, 50–56. [[CrossRef](#)] [[PubMed](#)]

6. Benek, O.; Korabecny, J.; Soukup, O. A Perspective on Multi-target Drugs for Alzheimer's Disease. *Trends Pharmacol. Sci.* **2020**, *41*, 434–445. [[CrossRef](#)]
7. Knopman, D.S.; Amieva, H.; Petersen, R.C.; Chételat, G.; Holtzman, D.M.; Hyman, B.T.; Nixon, R.A.; Jones, D.T. Alzheimer disease. *Nat. Rev. Dis. Prim.* **2021**, *7*, 33. [[CrossRef](#)] [[PubMed](#)]
8. Campora, M.; Francesconi, V.; Schenone, S.; Tasso, B.; Tonelli, M. Journey on Naphthoquinone and Anthraquinone Derivatives: New Insights in Alzheimer's Disease. *Pharmaceuticals* **2021**, *14*, 33. [[CrossRef](#)]
9. De Strooper, B.; Vassar, R.; Golde, T. The secretases: Enzymes with therapeutic potential in Alzheimer disease. *Nat. Rev. Neurol.* **2010**, *6*, 99–107. [[CrossRef](#)]
10. Huang, Y.; Potter, R.; Sigurdson, W.; Santacruz, A.; Shih, S.; Ju, Y.E.; Kasten, T.; Morris, J.C.; Mintun, M.; Duntley, S.; et al. Effects of age and amyloid deposition on Aβ dynamics in the human central nervous system. *Arch. Neurol.* **2012**, *69*, 51–58. [[CrossRef](#)]
11. Iwatsubo, T.; Odaka, A.; Suzuki, N.; Mizusawa, H.; Nukina, N.; Ihara, Y. Visualization of Aβ<sub>42</sub> and Aβ<sub>40</sub> in senile plaques with end-specific Aβ monoclonals: Evidence that an initially deposited species is Aβ<sub>42</sub>. *Neuron* **1994**, *13*, 45–53. [[CrossRef](#)] [[PubMed](#)]
12. Miller, D.L.; Papayannopoulos, I.A.; Styles, J.; Bobin, S.A.; Lin, Y.Y.; Biemann, K.; Iqbal, K. Peptide compositions of the cerebrovascular and senile plaque core amyloid deposits of Alzheimer's disease. *Arch. Biochem. Biophys.* **1993**, *301*, 41–52. [[CrossRef](#)] [[PubMed](#)]
13. Kodali, R.; Williams, A.D.; Chemuru, S.; Wetzel, R. Aβ<sub>1–40</sub> forms five distinct amyloid structures whose beta-sheet contents and fibril stabilities are correlated. *J. Mol. Biol.* **2010**, *401*, 503–517. [[CrossRef](#)] [[PubMed](#)]
14. Agopian, A.; Guo, Z. Structural origin of polymorphism of Alzheimer's amyloid beta-fibrils. *Biochem. J.* **2012**, *447*, 43–50. [[CrossRef](#)] [[PubMed](#)]
15. Petkova, A.T.; Leapman, R.D.; Guo, Z.; Yau, W.M.; Mattson, M.P.; Tycko, R. Self-propagating, molecular-level polymorphism in Alzheimer's beta-amyloid fibrils. *Science* **2005**, *307*, 262–265. [[CrossRef](#)] [[PubMed](#)]
16. Katzmarski, N.; Ziegler-Waldkirch, S.; Scheffler, N.; Witt, C.; Abou-Ajram, C.; Nuscher, B.; Prinz, M.; Haass, C.; Meyer-Luehmann, M. Aβ oligomers trigger and accelerate Aβ seeding. *Brain Pathol.* **2020**, *30*, 36–45. [[CrossRef](#)] [[PubMed](#)]
17. Srivastava, A.K.; Pittman, J.M.; Zerweck, J.; Venkata, B.S.; Moore, P.C.; Sachleben, J.R.; Meredith, S.C. Beta-Amyloid aggregation and heterogeneous nucleation. *Protein Sci.* **2019**, *28*, 1567–1581. [[CrossRef](#)] [[PubMed](#)]
18. Freysson, A.; Page, G.; Fauconneau, B.; Rioux Bilan, A. Natural polyphenols effects on protein aggregates in Alzheimer's and Parkinson's prion-like diseases. *Neural Regen. Res.* **2018**, *13*, 955–961. [[CrossRef](#)]
19. Jalili-Baleh, L.; Babaei, E.; Abdpour, S.; Nasir Abbas Bukhari, S.; Foroumadi, A.; Ramazani, A.; Sharifzadeh, M.; Abdollahi, M.; Khoobi, M. A review on flavonoid-based scaffolds as multi-target-directed ligands (MTDLs) for Alzheimer's disease. *Eur. J. Med. Chem.* **2018**, *152*, 570–589. [[CrossRef](#)] [[PubMed](#)]
20. Ullah, R.; Khan, M.; Shah, S.A.; Saeed, K.; Kim, M.O. Natural Antioxidant Anthocyanins—A Hidden Therapeutic Candidate in Metabolic Disorders with Major Focus in Neurodegeneration. *Nutrients* **2019**, *11*, 1195. [[CrossRef](#)]
21. Tena, N.; Martin, J.; Asuero, A.G. State of the Art of Anthocyanins: Antioxidant Activity, Sources, Bioavailability, and Therapeutic Effect in Human Health. *Antioxidants* **2020**, *9*, 451. [[CrossRef](#)]
22. Rupasinghe, H.P.V.; Arumuggam, N.; Amararathna, M.; De Silva, A.B.K.H. The potential health benefits of haskap (*Lonicera caerulea* L.): Role of cyanidin-3-O-glucoside. *J. Funct. Foods* **2018**, *44*, 24–39. [[CrossRef](#)]
23. Olivás-Aguirre, F.J.; Rodrigo-García, J.; Martínez-Ruiz, N.D.; Cardenas-Robles, A.I.; Mendoza-Díaz, S.O.; Alvarez-Parrilla, E.; González-Aguilar, G.A.; de la Rosa, L.A.; Ramos-Jiménez, A.; Wall-Medrano, A. Cyanidin-3-O-glucoside: Physical-Chemistry, Foodomics and Health Effects. *Molecules* **2016**, *21*, 1264. [[CrossRef](#)] [[PubMed](#)]
24. Meng, L.-s.; Li, B.; Li, D.-n.; Wang, Y.-h.; Lin, Y.; Meng, X.-j.; Sun, X.-y.; Liu, N. Cyanidin-3-O-glucoside attenuates amyloid-beta (1–40)-induced oxidative stress and apoptosis in SH-SY5Y cells through a Nrf2 mechanism. *J. Funct. Foods* **2017**, *38*, 474–485. [[CrossRef](#)]
25. Shin, W.-H.; Park, S.-J.; Kim, E.-J. Protective effect of anthocyanins in middle cerebral artery occlusion and reperfusion model of cerebral ischemia in rats. *Life Sci.* **2006**, *79*, 130–137. [[CrossRef](#)]
26. Andres-Lacueva, C.; Shukitt-Hale, B.; Galli, R.L.; Jauregui, O.; Lamuela-Raventós, R.M.; Joseph, J.A. Anthocyanins in aged blueberry-fed rats are found centrally and may enhance memory. *Nutr. Neurosci.* **2005**, *8*, 111–120. [[CrossRef](#)]
27. Liu, F.; Zhao, F.; Wang, W.; Sang, J.; Jia, L.; Li, L.; Lu, F. Cyanidin-3-O-glucoside inhibits Aβ<sub>40</sub> fibrillogenesis, disintegrates preformed fibrils, and reduces amyloid cytotoxicity. *Food Funct.* **2020**, *11*, 2573–2587. [[CrossRef](#)]
28. Chen, Y.; Chen, H.; Zhang, W.; Ding, Y.; Zhao, T.; Zhang, M.; Mao, G.; Feng, W.; Wu, X.; Yang, L. Bioaccessibility and biotransformation of anthocyanin monomers following in vitro simulated gastric-intestinal digestion and in vivo metabolism in rats. *Food Funct.* **2019**, *10*, 6052–6061. [[CrossRef](#)]
29. Walti, M.A.; Ravotti, F.; Arai, H.; Glabe, C.G.; Wall, J.S.; Bockmann, A.; Guntert, P.; Meier, B.H.; Riek, R. Atomic-resolution structure of a disease-relevant Aβ<sub>1–42</sub> amyloid fibril. *Proc. Natl. Acad. Sci. USA* **2016**, *113*, E4976–E4984. [[CrossRef](#)]
30. Gao, J.; Yu, P.; Liang, H.; Fu, J.; Luo, Z.; Yang, D. The wPDI Redox Cycle Coupled Conformational Change of the Repetitive Domain of the HMW-GS 1Dx5-A Computational Study. *Molecules* **2020**, *25*, 4393. [[CrossRef](#)]
31. Yu, P.; Zhou, F.; Yang, D. Curdlan conformation change during its hydrolysis by multi-domain beta-1,3-glucanases. *Food Chem.* **2019**, *287*, 20–27. [[CrossRef](#)] [[PubMed](#)]

32. Choi, E.Y.; Kang, S.S.; Lee, S.K.; Han, B.H. Polyphenolic Biflavonoids Inhibit Amyloid-Beta Fibrillation and Disaggregate Preformed Amyloid-Beta Fibrils. *Biomol. Ther.* **2020**, *28*, 145–151. [[CrossRef](#)] [[PubMed](#)]
33. Baumketner, A.; Bernstein, S.L.; Wyttenbach, T.; Bitan, G.; Teplow, D.B.; Bowers, M.T.; Shea, J.E. Amyloid  $\beta$ -protein monomer structure: A computational and experimental study. *J. Protein Sci.* **2006**, *15*, 420–428. [[CrossRef](#)] [[PubMed](#)]
34. Lazo, N.D.; Grant, M.A.; Condrón, M.C.; Rigby, A.C.; Teplow, D.B. On the nucleation of amyloid  $\beta$ -protein monomer folding. *J. Protein Sci.* **2005**, *14*, 1581–1596. [[CrossRef](#)] [[PubMed](#)]

**Disclaimer/Publisher’s Note:** The statements, opinions and data contained in all publications are solely those of the individual author(s) and contributor(s) and not of MDPI and/or the editor(s). MDPI and/or the editor(s) disclaim responsibility for any injury to people or property resulting from any ideas, methods, instructions or products referred to in the content.